Design and Implementation of a ZCS Two-Switch Forward Converter with Variable inductor

P. T. Chen T. J. Liang L. S. Yang M. Y. Cheng S.M. Chen

Green Energy Electronics Research Center
Department of Electrical Engineering, National Cheng-Kung University, Taiwan.
tjliang@mail.ncku.edu.tw

***Abstract* – A zero-current-switching (ZCS) two-switch DC-DC forward converter with variable-inductor is presented in this paper. The quasi-resonant technique is employed to achieve ZCS operation. This variable inductor technique is used to reduce the switching losses and the peak value of the output-diode current. Thus, the conversion efficiency can be improved. Moreover, the voltage across the active switch is clamped at the DC-source input voltage. So, the voltage stress of the active switch is less than that of the conventional DC-DC forward converter. Finally, a prototype circuit is implemented to verify the performance.**

***Index Terms* —two-switch forward converter, variable inductor, ZCS, quasi-resonant**

I. INTRODUCTION

Since power supplies are used widely in the electronic products, large power density is very important. Conventional linear power supplies have some advantages, such as low output ripples, high reliability, and low electro-magnetic interference, but their disadvantages are low power density and low conversion efficiency. Therefore, the switching power supplies are being researched for their ability to increase power density and conversion efficiency. Some switching power supplies utilize pulse-width modulation (PWM) technique, but this approach results in large switching losses [1, 2]. In order to reduce the switching losses, soft-switching techniques, such as resonant and quasi-resonant topologies, are developed [3]-[9]. The LC resonant tank is employed for these topologies to achieve zero-current switching (ZCS) or zero-voltage switching (ZVS) for the power devices. Thus, the switching losses can be reduced. However, since the switching frequency of these topologies is not fixed, it will result in higher current stress and conduction losses at the heavy-load condition. Therefore, a variable inductor is used in the resonant tank to adjust the switching frequency for different loads [10]-[13].

A ZCS two-switch DC-DC forward converter is presented in this paper. The variable inductor in the resonant bank is used to reduce the switching losses and peak value of the output-diode current. A prototype circuit with input voltage 400 V, output voltage 48 V, and output power 384 W is implemented to verify the performance.

II. OPERATING PRINCIPLES OF THE PROPOSED CONVERTER

Fig. 1 shows the circuit configuration of the proposed converter, which consists of two switches (S_1 and S_2), one transformer, four diodes (D_1, D_2, D_o and D_f), one resonant tank (L_r – C_r), one output inductor (L_o), and one output capacitor (C_o). Switches S_1 and S_2 are controlled by the same gate-drive signal. Variable inductor L_r is employed for the resonant inductor. The resonant tank is used to achieve ZCS when the switches are turned off. The switching frequency is varied to regulate the output voltage. The turns ratio of transformer n is equal to N_s/N_p.

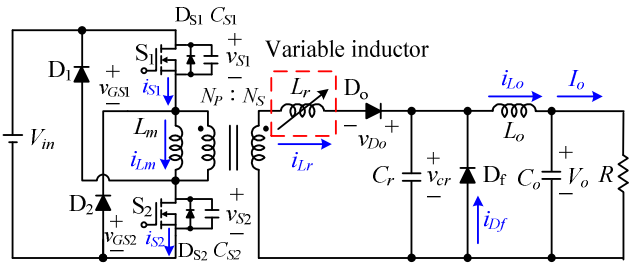

Fig. 1. Circuit configuration of the proposed converter.

In order to simplify the analysis, the following assumptions are made:

- The leakage inductor and the stray capacitor of the transformer are neglected.
- The output inductor is large enough that the current through the output inductor can be treated as constant during one switching period.
- The output capacitor is large enough that the voltage across the output capacitor can be treated as constant during one switching period.
- The output inductor and output capacitor are larger than the resonant inductor and resonant capacitor.
- All the components are ideal.

The key waveforms of the proposed converter are shown in Fig. 2. The operating principle of the proposed converter is described as follows.

Mode I [t_0 , t_1]:

At $t = t_0$, S_1 and S_2 are turned on. The current-flow path is shown in Fig. 3(a). The DC-source energy is transferred to

the resonant tank via the transformer. Meanwhile, v_{cr} is equal to zero. So, the voltage across L_r is given as

$$v_{Lr}(t) = nV_{in} = L_r \frac{di_{Lr}(t)}{dt} \quad (1)$$

Since i_{Lr} is equal to I_o at $t = t_1$, the following equation is obtained as

$$nV_{in} = \frac{L_r I_o}{t_1 - t_0} \quad (2)$$

Thus, the duration $[t_0, t_1]$ is found to be

$$t_1 - t_0 = \frac{L_r I_o}{nV_{in}} \quad (3)$$

Mode II [t_1, t_2]:
At $t = t_1$, S_1 and S_2 are still turned on. The current flow path is shown in Fig. 3(b). The resonant tank starts to resonate between L_r and C_r, and the following exist:

$$v_{cr}(t) = nV_{in} - L_r \frac{di_{Lr}(t)}{dt}, \quad t_1 \le t \le t_2 \quad (4)$$

$$i_{cr}(t) = i_{Lr}(t) - I_o, \quad t_1 \le t \le t_2 \quad (5)$$

Substituting $i_{Lr}(t_1) = I_o$ into (4) and (5), i_{Lr} and v_{cr} are found to be

$$v_{cr}(t) = nV_{in}\left[1 - \cos\omega(t - t_1)\right], \quad t_1 \le t \le t_2 \quad (6)$$

$$i_{Lr}(t) = I_o + \frac{nV_{in}}{Z_n}\sin\omega(t - t_1), \quad t_1 \le t \le t_2 \quad (7)$$

where $\omega = 1/\sqrt{L_r C_r} = 2\pi f_r$ and $Z_n = \sqrt{L_r / C_r}$.
From (6) and (7), the peak values of v_{cr} and i_{Lr} are derived as

$$V_{cr\_peak} = 2nV_{in} \quad (8)$$

$$I_{Lr\_peak} = I_o + \frac{nV_{in}}{Z_n} \quad (9)$$

Fig. 2 shows that i_{Lr} is equal to zero at $t = t_2$. Substituting $i_{Lr}(t_2) = 0$ into (7) yields the following:

$$I_o + \frac{nV_{in}}{Z_n}\sin\omega(t_2 - t_1) = 0 \quad (10)$$

Therefore, the duration $[t_1, t_2]$ is given by

$$t_2 - t_1 = \frac{1}{\omega}\sin^{-1}\left(-\frac{I_o Z_n}{nV_{in}}\right) \quad (11)$$

Mode III [t_2, t_3]:
At $t = t_2$, S_1 and S_2 are still turned on. The current-flow path is shown in Fig. 3(c). Meanwhile, there is no energy stored in L_r. The energy stored in C_r is delivered to L_o, C_o, and the load. Thus, i_{cr} is given as

$$i_{cr}(t) = C_r \frac{dv_{cr}(t)}{dt} \quad (12)$$

Mode IV [t_3, t_4]:
At $t = t_3$, S_1 and S_2 are turned off. The current-flow path is shown in Fig. 3(d). The energy of the DC-source and L_m are transferred to C_{S1} and C_{S2}. The energy stored in C_r is still discharged to L_o, C_o, and the load. At $t = t_4$, v_{cr} is equal to zero, and this mode ends. Since i_{cr} is equal to I_o at this time interval $[t_2, t_4]$, (12) can be rewritten as

$$I_o = \frac{C_r v_{cr}(t_2)}{t_4 - t_2} \quad (13)$$

At $t = t_2$, (6) can be represented as

$$v_{cr}(t_2) = nV_{in}[1 - \cos\omega(t_2 - t_1)] \quad (14)$$

So, the duration $[t_2, t_4]$ is obtained as

$$t_4 - t_2 = \frac{nC_r V_{in}}{I_o}[1 - \cos\omega(t_2 - t_1)] \quad (15)$$

Mode V [t_4, t_5]:
During this mode, S_1 and S_2 are still turned off. The current-flow path is shown in Fig. 3(e). The energy of the DC-source and L_m are still transferred to C_{S1} and C_{S2}. The energy stored in L_o is released to C_o and the load. When the voltages across C_{S1} and C_{S2} are equal to V_{in} at $t = t_5$, this mode ends.

Mode VI [t_5, t_6]:
At this mode, S_1 and S_2 are still turned off. The current-flow path is shown in Fig. 3(f). The energy stored in L_m is entirely released to the DC-source through D_1 and D_2 and the voltages across S_1 and S_2 are clamped at V_{in}. The energy stored in L_o is still released to C_o and the load.

Mode VII [t_6, t_7]:
At this mode, S_1 and S_2 are still turned off. The current flow path is shown in Fig. 3(g). Since the energy stored in L_m is released to empty at $t = t_6$, the energies stored in C_{S1} and C_{S2} are discharged to L_m and the DC-source. The energy stored in L_o is still released to C_o and the load. When the voltages across C_{S1} and C_{S2} are equal to $0.5V_{in}$ at $t = t_7$, this mode ends.

Mode VIII [t_7, t_8]:
At this mode, S_1 and S_2 are still turned off. The current-flow path is shown in Fig. 3(h). The energy stored in L_m is released to the DC source through D_{S1} and D_{S2} until $i_{Lm} = 0$. The energy stored in L_o is still released to C_o and the load. Then, the next switching period begins.

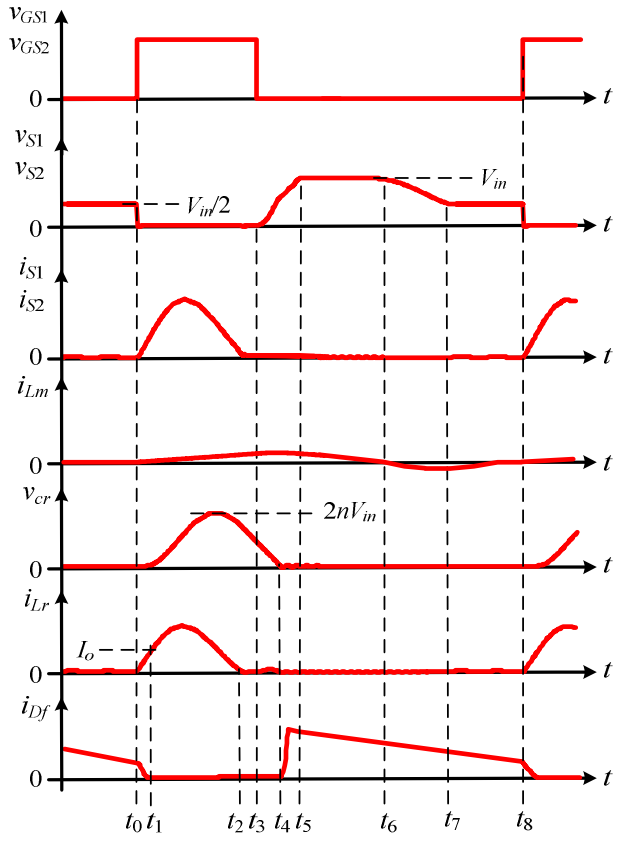

Fig. 2. The key waveforms of the proposed converter.

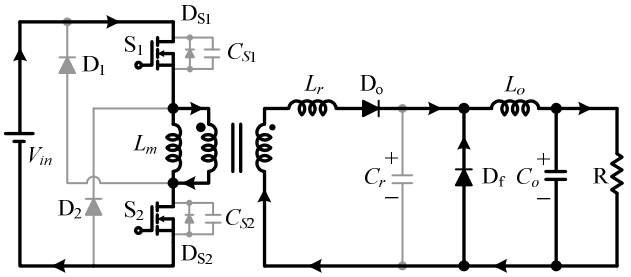

(a)

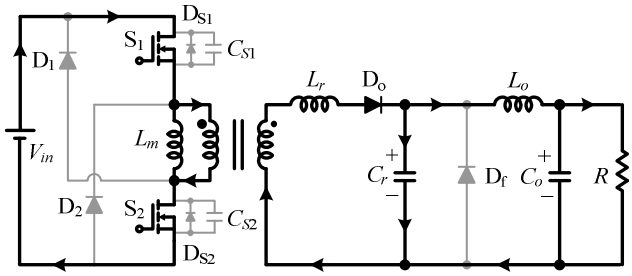

(b)

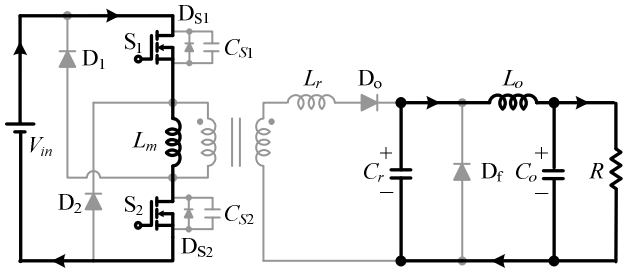

(c)

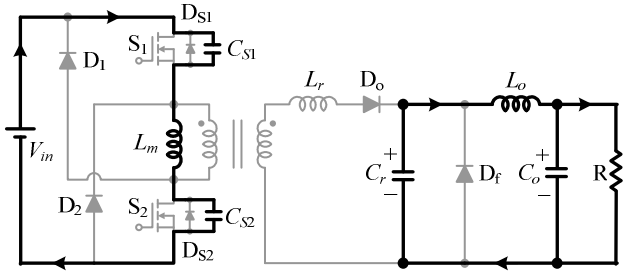

(d)

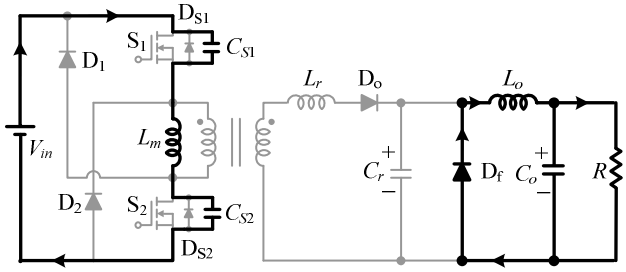

(e)

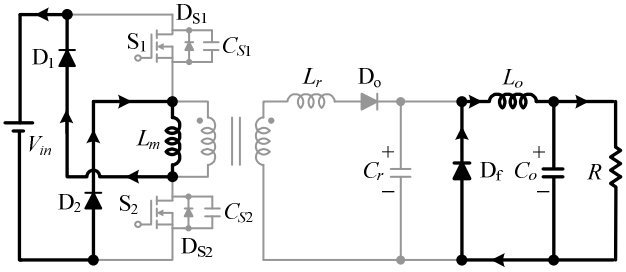

(f)

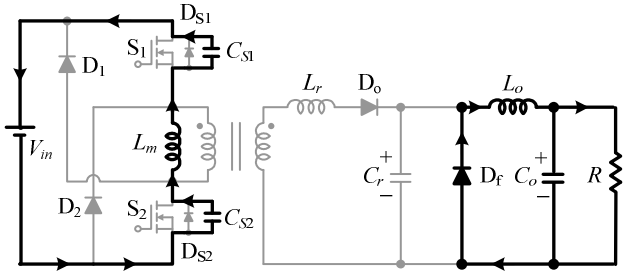

(g)

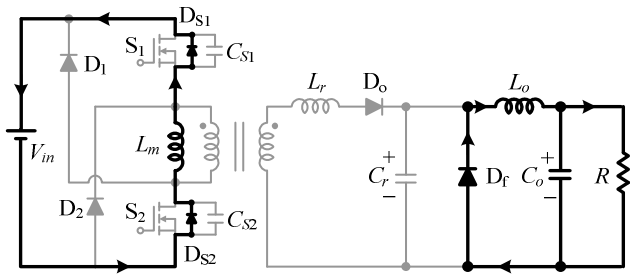

(h)

Fig. 3. Current flow path of operating modes during one switching period.

III. Steady-State Analysis of the Proposed Converter

Assuming all device components are ideal, the input energy is given as

$$W_{in}=\int_0^{t_3} V_{in} i_{in} dt = nV_{in}I_o\left[\frac{1}{2}(t_1-t_0)+(t_2-t_1)+(t_4-t_2)\right] \quad (16)$$

The output energy is derived as

$$W_o=\int_0^{T_S} V_o I_o dt = V_o I_o T_S \quad (17)$$

From (16) and (17), the output voltage V_o is found to be

$$V_o=\frac{nV_{in}}{T_S}\left[\frac{1}{2}(t_1-t_0)+(t_2-t_1)+(t_4-t_2)\right] \quad (18)$$

Substituting (3), (11) and (15) into (18) yields

$$V_o=\frac{nV_{in}}{T_S}\{\frac{L_r I_o}{2nV_{in}}+\frac{1}{\omega}\sin^{-1}(-\frac{I_o Z_n}{nV_{in}}) +\frac{C_r nV_{in}}{I_o}[1-\cos\omega(t_2-t_1)]\} \quad (19)$$

The normalized parameters are defined as follows:

Normalized voltage: $V_n=\frac{V_o}{nV_{in}}$ (20)

Normalized frequency: $f_n=\frac{f_s}{f_r}$ (21)

Normalized impedance: $r_n=\frac{R}{Z_n}$ (22)

Substituting (20) – (22) into (19) yields following equation:

$$V_n-\frac{f_n}{2\pi}\left\{\frac{V_n}{2r_n}+\sin^{-1}(\frac{-V_n}{r_n})+\frac{r_n}{V_n}\left[1+\sqrt{1-(\frac{V_n}{r_n})^2}\right]\right\}=0 \quad (23)$$

The relationship between normalized output voltage V_n and normalized switching frequency f_n is shown in Fig. 4. When parameters V_n, f_n, and Z_n are selected, the switching frequency can be regulated to control the output voltage.

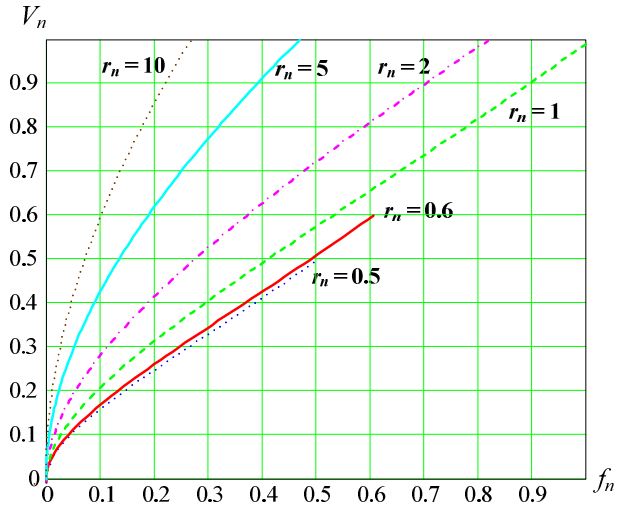

Fig. 4. Normalized output voltage V_n versus normalized switching frequency f_n.

IV. Experimental Results

A laboratory prototype circuit is implemented to illustrate the performance of the proposed converter. The circuit specifications and parameters are selected to be V_{in} = 400 V, V_o = 48 V, P_o = 384 W, n = 0.2, $f_{s,max}$ = 100 kHz, and C_r = 220 nF. Moreover, the power devices are chosen as S_1/S_2: STP20NM60, D_1/D_2: UF4006, and D_o/D_f: MBR20200CT.

Fig. 5 shows the control circuit of the variable-inductor. Resistor R_X is used to detect the output current and the comparator detects the voltage drop on R_X. If the output current is larger than 4 A, the output level of the comparator decreases to a low level. Then, switch S_X is turned off. Thus, the inductance of L_r can be adjusted as shown in Fig. 6.

Figs. 7 and 8 show some experimental waveforms at the full-load condition, P_o = 384 W. As shown in Fig. 7, switch S_1 is turned off at i_{S1} = 0. Thus, ZCS operation of the proposed converter is achieved. Fig. 8(a) depicts that when the inductance of L_r is variable, f_s is 106 kHz and the peak value of i_{Lr} is 22 A. Fig. 8(b) shows that f_s is 129 kHz and the peak value of i_{Lr} is 25.6 A under L_r = 3.2 μH. Thus, the variable-inductor technique can effectively reduce the switching losses and peak value of output-diode current. Fig. 9 shows the measured efficiency, and it is clear that the variable-inductor technique is better than the fixed-inductance technique at heavy-load conditions. Also, the maximum efficiency of the proposed converter is 93.3 % at P_o = 288 W.

V. Conclusions

A ZCS two-switch DC-DC forward converter with variable inductor is researched in this paper. The proposed converter employs a quasi-resonant technique to achieve ZCS

operation. A variable-inductor technique is used to reduce the switching losses and peak value of the output-diode current, and the extra third winding in the transformer is not required. The residual energy of the transformer can be delivered to the DC source. Moreover, the voltages across switches S_1 and S_2 can be clamped at DC-source voltage V_{in}. Finally, a prototype circuit is implemented. Experimental results shown that the maximum efficiency is 93.3 % at P_o = 288 W.

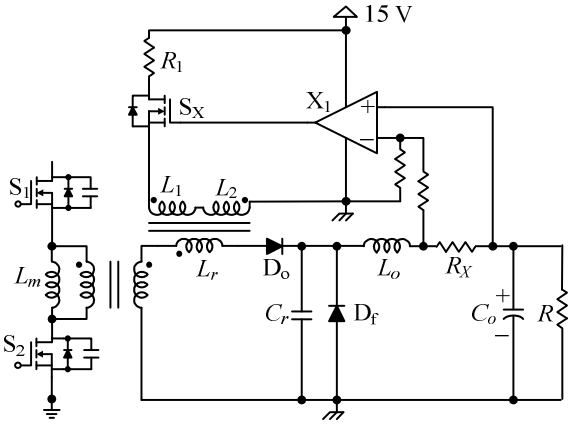

Fig. 5. Control circuit of variable inductor.

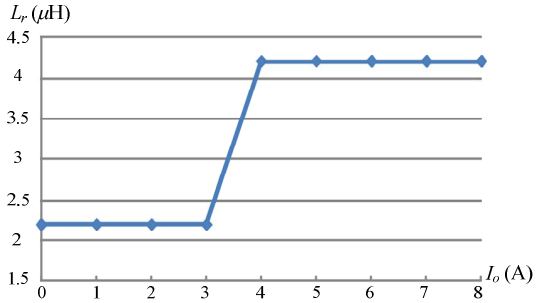

Fig. 6. Inductance of L_r versus output current.

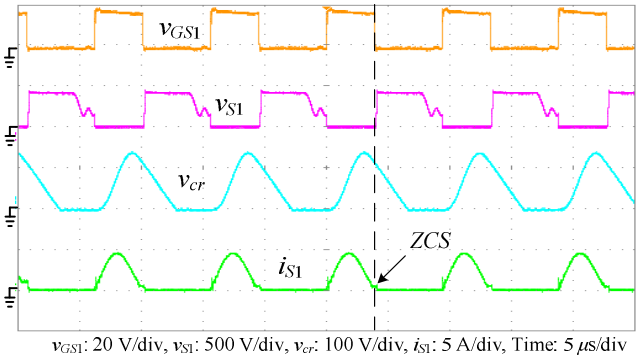

v_{GS1}: 20 V/div, v_{S1}: 500 V/div, v_{cr}: 100 V/div, i_{S1}: 5 A/div, Time: 5 μs/div

Fig. 7. Waveforms of v_{GS1}, v_{S1}, v_{cr}, and i_{S1} at P_o = 384 W.

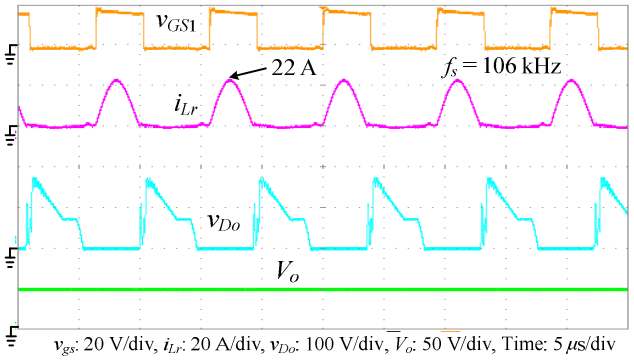

v_{gs}: 20 V/div, i_{Lr}: 20 A/div, v_{Do}: 100 V/div, V_o: 50 V/div, Time: 5 μs/div

(a)

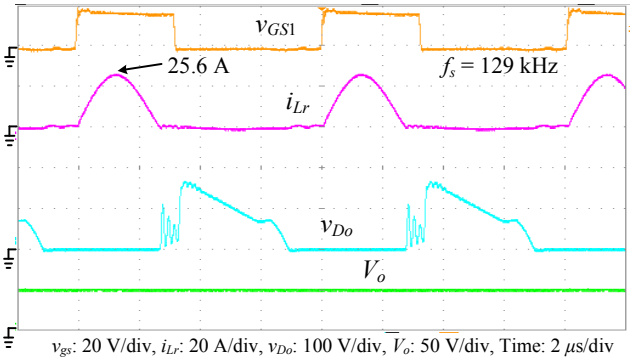

v_{gs}: 20 V/div, i_{Lr}: 20 A/div, v_{Do}: 100 V/div, V_o: 50 V/div, Time: 2 μs/div

(b)

Fig. 8 Waveforms of v_{GS1}, i_{Lr}, v_{Do}, and V_o at P_o = 384 W: (a) variable inductance L_r, (b) L_r = 3.2 μH.

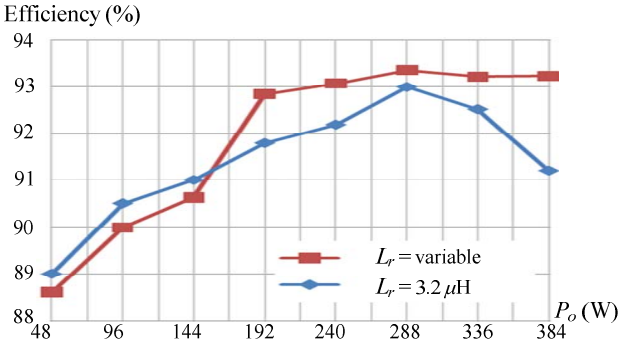

Fig. 9 Measured efficiency under various load.

ACKNOWLEDGMENT

The authors gratefully acknowledge financial support from the National Science Council of Taiwan under project No. NSC 98-2221-E-006-247-MY3 as well as from the Research Center of Ocean Environment and Technology of National Cheng Kung University.

REFERENCES

[1] F. D. Tan, "The forward converter: from the classic to the contemporary," *IEEE APEC*, pp. 857-863, 2002.

[2] D. J. Ionel and C. George, "High efficiency DC-DC converter," *IEEE APEC*, pp. 638-644, 1994.

[3] K. Chen and T. A. Stuart, "A study of IGBT turn-off behavior and switching losses for zero-voltage and zero-current switching," *IEEE APEC*, pp. 411-418, 1992.
[4] Z. Yang and P. C. Sen, "Recent Developments in High Power Factor Switch-Mode Converters," *IEEE Proc. on ECE*, vol. 2, pp. 477-480, May 1998.
[5] F. S. Tsai and F. C. Lee, "A complete DC characterization of a constant-frequency, clamped-mode, series-resonant inverter for induction heating," *IEEE PESC*, pp. 450-456, 1995.
[6] F. C. Lee, "High-frequency quasi-resonant converter technologies," *IEEE Invited Paper*, vol. 76, no. 4, pp. 377-390, Apr. 1988.
[7] I. Barbi, J. C. O. Balacell, D. C. Martins, and F. B. Libano, "Buck quasi-resonant converter operating at constant frequency analysis, design and experimentation," *IEEE Trans. on Power Electronics*, vol. 5, no. 3, pp.276-283, Jul. 1990.
[8] J. Xu, V. Caliskan, and C.Q. Lee, "Transient time-domain analysis of zero-current switching quasi-resonant converters," *IEEE APEC*, pp. 1028-1034, 1994.
[9] R. J. Wai, C. Y. Lin, L. W. Liu, and R. Y. Duan, "Voltage-clamped forward quasi-resonant converter with soft switching and reduced switch stress," *IEE Proc. on Electric Power Applications*, vol. 152, pp. 558-564, May 2005.
[10] D. Medini and S. Ben-Yaakov, "A current-controlled variable-inductor for high frequency resonant power circuits," *IEEE APEC*, vol. 1, pp. 219-225, 1994.
[11] J.-U. W. Hsu, A. P. Hu, A. Swain, Xin Dai and Yue Sun, "A new contactless power pick-up with continuous variable inductor control using magnetic amplifier," *IEEE Proc. on Power con*, pp. 1-8, 2006.
[12] M. S. Perdigao, J. M. Alonso, M. A. Dalla Costa, and E. S. Saraiva, "A variable inductor MATLAB/Simulink behavioral model for application in magnetically controlled electronic ballasts," Power Electronics, Electrical Drives, Automation and Motion, pp.349-354, Jun. 1994.
[13] J. M. Alonso, M. A. Dalla Costa, M. Rico-Secades, J. Cardesin and J. Garcia, "Investigation of a new control strategy for electronic ballasts based on variable inductor, " *IEEE Trans. on Power Electronics*, vol. 55, no. 1, pp. 3-10, Jan. 2008.